Quantum interference and heteroaromaticity of *para*- and *meta*-linked bridged biphenyl units in single molecular conductance measurements

Markus Gantenbein[1], Lin Wang[2,7,8], Alaa A. Al-jobory[3,4], Ali K. Ismael[3,5], Colin J. Lambert[3], Wenjing Hong[6,2] & Martin R. Bryce[1]

Is there a correlation between the (hetero)aromaticity of the core of a molecule and its conductance in a single molecular junction? To address this question, which is of fundamental interest in molecular electronics, oligo(arylene-ethynylene) (OAE) molecular wires have been synthesized with core units comprising dibenzothiophene, carbazole, dibenzofuran and fluorene. The biphenyl core has been studied for comparison. Two isomeric series have been obtained with 4-ethynylpyridine units linked to the core either at *para-para* positions (*para* series **1–5**) or *meta-meta* positions (*meta* series **6–10**). A combined experimental and computational study, using mechanically controlled break junction measurements and density functional theory calculations, demonstrates consistently higher conductance in the *para* series compared to the *meta* series: this is in agreement with increased conjugation of the π–system in the *para* series. Within the *para* series conductance increases in the order of decreasing heteroaromaticity (dibenzothiophene < carbazole < dibenzofuran). However, the sequence is very different in the *meta* series, where dibenzothiophene ≈ dibenzofuran < carbazole. Excellent agreement between theoretical and experimental conductance values is obtained. Our study establishes that both quantum interference and heteroaromaticity in the molecular core units play important and inter-related roles in determining the conductance of single molecular junctions.

[1]Department of Chemistry, Durham University, Durham DH1 3LE, UK.
[2]Department of Chemistry and Biochemistry, University of Bern, Freiestrasse 3, Bern CH-3012, Switzerland.
[3]Department of Physics, Lancaster University, Lancaster LA1 4YB, UK.
[4]Department of Physics, College of Education for Pure Science, Anbar University, Anbar, Iraq.
[5]Department of Physics, College of Education for Pure Science, Tikrit University, Tikrit, Iraq.
[6]Collaborative Innovation Center of Chemistry for Energy Materials, Department Chemical and Biochemical Engineering, College of Chemistry and Chemical Engineering, Xiamen University, Xiamen 361005, China.
[7]Key Laboratory of Molecular Nanostructure and Nanotechnology, Institute of Chemistry Chinese Academy of Sciences, Beijing 100190, China.
[8]University of the Chinese Academy of Sciences, Beijing, China.

The measurement and understanding of charge transport in single molecules is of fundamental interest and is relevant to the proposed future applications of molecules in electronic devices[1–6]. Many studies have addressed correlations between molecular structure and transport properties of molecules wired into metal–molecule–metal nanoscale junctions[7,8]. Several experimental approaches are well established for measuring transport through single (or a few) molecules, notably the mechanically controlled break junction (MCBJ)[9] and scanning tunnelling microscopy-break junction (STM-BJ) techniques[10]. Combined experimental and theoretical studies[11] have established that charge transport through molecular junctions is controlled by the intrinsic properties of the molecular backbone, the terminal anchoring group, and the metal leads. Key features are the molecular length, the molecular conformation, the gap between the highest occupied and the lowest unoccupied molecular orbitals (the HOMO-LUMO gap), the alignment of this gap to the Fermi level of the metal electrodes, and the coordination geometry at the metal-molecule contacts. Oligo(arylene-ethynylene) (OAE)-type molecular wires have been widely explored in single molecular junctions[12–16]. They are π–conjugated, rod-like molecules and their functional properties can be systematically tuned over a wide range of parameters by chemical synthesis[17].

In the present work we investigate a series of ten OAE molecules **1**–**10** whose structures are shown in Figure 1. The molecular design combines three key structural features: (i) all of the molecules have terminal pyridyl anchoring units at both ends; (ii) each molecule has one of five different core units and (iii) there is either *para-para* or *meta-meta* conjugation through the core unit, providing two isomeric series. The dibenzothiophene (**1**, **6**), *N*-ethylcarbazole (**2**, **7**), dibenzofuran (**3**, **8**) and 9,9-dimethylfluorene cores (**4**, **9**) are rigid and planar. Heteroaromaticity, i.e., the resonance energy, will decrease in the sequence dibenzothiophene > carbazole > dibenzofuran, reflecting the extent of delocalization of a lone pair from the heteroatom into the π–system of the central ring (S > N > O)[18]. Fluorene, with no heteroatom and a bridging sp^3 carbon atom instead, has a non-aromatic central ring. In contrast to the other molecules in Figure 1, biphenyl derivatives **5** and **10** possess a flexible and twisted core. It is well known that increasing the torsion angle within a biphenyl unit leads to reduced single-molecule conductance[19–23], therefore, **5** and **10** are studied here as model compounds.

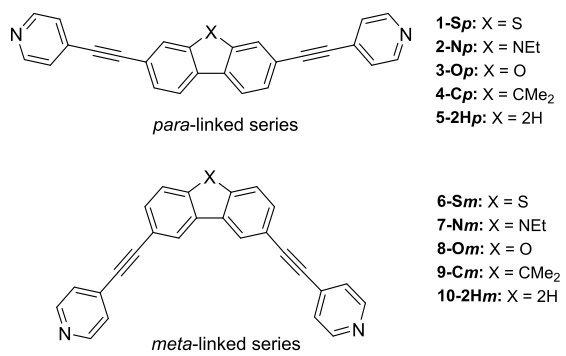

Figure 1 | Structures of the molecules discussed in this work and their nomenclature. The structures represent the *para*-linked series **1–5** (top) and *meta*-linked series **6–10** (bottom)

We are aware of only two related reports on the effect of heteroaromaticity on single-molecule conductance. Venkataraman, Breslow and co-workers studied three amine-terminated molecules comprising thiophene, furan and dimethylcyclopentadiene cores (**11–13**, Figure 2). Based on STM–BJ measurements the authors concluded that aromaticity in the core leads to a decrease in the single-molecule conductance, i.e. the non-aromatic cyclopentadiene derivative **13** has the highest conductance, while the most aromatic thiophene derivative **11** has

the lowest conductance[24]. This work did not consider the linkage of the anchor units to different positions on the core.

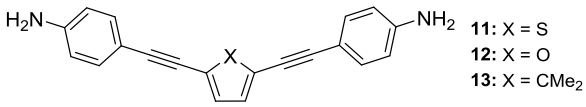

Figure 2| Molecules studied in reference 23. Amine-terminated molecules **11–13** measured by STM-BJ.

A second study concerns multiple pathways through a molecular wire based on fluorene-like molecules[25]. Several studies have established that *para* (conjugated) connectivity through a core unit results in enhanced conductance compared to the isomeric *meta* (reduced conjugation) connectivity. This is ascribed to quantum interference and has been observed experimentally and theoretically in aromatic rings such as benzene[26–29], naphthalene[14], anthracene[14], pyrene[30] and anthanthrene[31].

The motivation for the present work is to study for the first time the combined effects of two important molecular parameters on the single-molecule conductance of molecular wires: (i) heteroaromaticity in the core of the wire, and (ii) *para* versus *meta* conjugation through the core unit.

Results

Synthesis. For the synthesis of the *para*-linked **1–5** and *meta*-linked **6–10** molecules (Scheme 1) a tandem two-pot reaction sequence was followed. To enable the Sonogashira cross coupling of the corresponding aryldibromide central units (structures **14–23**[32–39] in SI) at elevated temperatures, desilylation of 4-((tri-methyl-silyl)ethynyl)pyridine[40] with TBAF (1 M in THF) was performed in 1,4-dioxane (room temperature for 30 min). Since the light-sensitive 4-ethynylpyridine is not stable in air, the mixture was directly subjected to the aryldibromide in the presence of $PdCl_2(PhCN)_2$, CuI, *t*-Bu_3P, and $(i\text{-}Pr)_2NH$, to give the target structures **1–10** in very good yields (Schemes S1 and S2). All the compounds were characterized by ^1H and ^{13}C NMR spectroscopy, mass spectrometry and elemental analysis. In addition, to assess the extent of conjugation within compounds **1–10** their UV–Vis absorption spectra were measured in a dilute and aerated dichloromethane solution at room temperature (Supplementary Figure 1). The optical HOMO-LUMO gaps (E_g) were calculated from the onset of the absorption and are listed in Supplementary Table 1. Compounds **1–5**, with the anchor groups attached in the *para* positions, show a smaller HOMO–LUMO gap compared to the *meta* isomers **6-10**. This is consistent with reduced conjugation in the *meta* series.

Single-molecule Conductance Measurements. Single-molecule conductance measurements of **1–10** in molecular junctions were performed using a home-built mechanically controllable break junction (MCBJ) setup at a bias V_{bias} = 0.1 V. Figure 3a shows typical individual conductance G (in units of quantum point conductance $G_0=2e^2/h$) versus distance (Δz) stretching traces in the measurement of **N*p***. The conductance in the molecule-free traces (black line) reveals exponential decrease characteristics upon the stretching process. When molecule **N*p*** is present a pronounced conductance plateau around 10^{-5} G_0 could be detected (green line) after the Au–Au contact breaks, which is assigned to the gold–molecule–gold junction. Since the break junction method can create a large number of molecular junctions with different molecule–electrode contact geometries, more than 1000 curves were recorded for statistical analysis to determine the most probable conductance of the molecular junctions. We further introduced a relative distance (Δz) and defined Δz = 0 at 0.5 G_0 to align all the traces. This

procedure leads to an accurate alignment of the conductance−distance traces because of the sharp drop in conductance at $G < G_0$. The electrode separation z_{exp} is then estimated by $z_{exp} = \Delta z + \Delta z_{corr}$, where $\Delta z_{corr} = 0.5 \pm 0.1$ nm corresponds to the "snap-back" nanogap which forms immediately upon breaking of the gold-gold atomic contact[41]. The all–data two–dimensional (2D) histogram (Figure 3b) exhibits features of gold–gold contacts around $G \geq 1\ G_0$, followed by another well-defined conductance scatter group in the range of $10^{-4}\ G_0 \sim 10^{-6}\ G_0$ which is attributed to the formation of single–molecule junctions. Figures 3c-d demonstrate the comparison between molecules with different heteroatoms and anchoring positions. For the compounds **1–3** with the *para–para* connectivity, the conductance clearly increases in the sequence **S*p*** < **N*p*** < **O*p***. However, for the isomers **6–8** where the anchoring groups are attached at *meta–meta* positions, the conductance reveals a different trend, **S*m*** ≈ **O*m*** < **N*m***. Control experiments using analogues with a carbon bridge (**4-C*p*** and **9-C*m***) and without any bridging atom (**5-2H*p*** and **10-2H*m***) were also conducted. The conductance of **2H*m*** could not be measured within the detection range of our setup. This can be explained by the *meta* coupling combined with a non-planar biphenyl core giving a conductance value below the direct tunneling conductance[29].

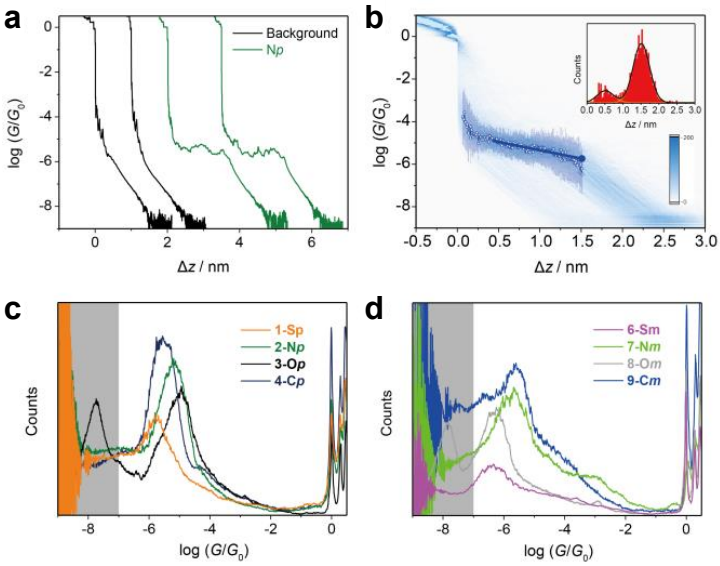

Figure 3 | Single-molecule conductance results from MCBJ experiments. (**a**) Typical individual conductance–distance traces (horizontally offset for clarity) of **N*p*** (green) and pure tunneling traces (black). (**b**) All-data-point 2D conductance versus relative distance (Δ*z*) of **N*p***. In 2D histogram, statistically averaged conductance−distance traces (hollow circles) with variations indicated by the standard deviations (bars) are shown, along with the linear fit (line). The solid circle represents the last data point in the linear fit before junction rupture. Inset: Stretching distance distribution obtained between $10^{-0.30}\ G_0$ and $10^{-6.25}\ G_0$. (**c**) and (**d**) All-data-point 1D conductance histograms constructed from more than 1,000 MCBJ traces of molecules with anchoring groups on (**c**) *para-para* and (**d**) *meta–meta* position. The gray area represents the detection limit of the MCBJ set up at $10^{-7}\ G_0$.

As the junction configuration is known to have a significant effect on the single–molecule conductance, we further explored the master curves composed of the fitted conductance with standard variation at each cross-sectional distance point[42]. After a linear fitting, the **N*p*** junction conductance with a fully stretched molecular conformation before the junction rupture can be deduced as $10^{-5.74 \pm 0.17}\ G_0$, which should be closer to the theoretical predicted configurations.

Table 1 | Most Probable Conductance Values as Obtained from MCBJ Experiments and Computations.

Compound	MCBJ ($\log(G/G_0)$)[a]		DFT ($\log(G/G_0)$)[b]		$G_{F\,para}$–$G_{F\,meta}$ ($\log(G/G_0)$)[c]		JFP (%)[d]	Electrode separation $z_{exp} = \Delta z + \Delta z_{corr}$ (nm)[e]	Theoretical length (nm)
	G_M[a]	G_F[b]	G_M[a]	G_F[b]	MCBJ	DFT			
1-S*p*	–5.79 ± 0.30	–5.93 ± 0.16	–5.50	–5.74	0.72	0.66	69	2.04 ± 0.45	2.04
2-N*p*	–5.22 ± 0.40	–5.74 ± 0.17	–5.15	–5.36	0.67	0.70	83	2.01 ± 0.23	2.02
3-O*p*	–5.04 ± 0.47	–5.47 ± 0.22	–5.10	–5.33	1.37	1.19	99	1.92 ± 0.26	2.03
4-C*p*	–5.55 ± 0.44	–5.81 ± 0.12	–5.44	–5.66	0.09	0.68	70	1.84 ± 0.22	2.03
5-2H*p*	–5.40 ± 0.36	–5.68 ± 0.11	–5.30	–5.55	>1.32	2.34	83	2.11 ± 0.23	2.08
6-S*m*	–6.34 ± 0.47	–6.65 ± 0.35	–6.34	–6.40			100	1.64 ± 0.29	1.51
7-N*m*	–5.76 ± 0.48	–6.41 ± 0.25	–6.06	–6.06			71	1.66 ± 0.14	1.56
8-O*m*	–6.32 ± 0.38	–6.84 ± 0.24	–6.40	–6.52			100	1.65 ± 0.19	1.55
9-C*m*	–5.66 ± 0.82	–5.90 ± 0.39	–5.74	–6.34			100	1.46 ± 0.29	1.51
10-2H*m*	< –7	< –7	–7.38	–7.89			–	–	1.41

[a]Conductance fitted by Gaussian function in the 1D histogram. [b]Molecular conductance through fully stretched junction obtained by linear fitting of the master curve. [c]Fully-stretched conductance difference between *para*- and *meta*-linked molecule for each heteroatom. [d]Junction formation probability judged by area ratio of the peak in the plateau length distribution. [e]Most-probable electrode separation at the end of conductance plateau. Error bars are based on the Gaussian fitting of conductance all-data-point 1D histogram and plateau displacement distribution.

It is found that there is some difference in the conductance comparison among different molecules: **O*m*** shows lower conductance than **S*m*** for the conductance of the fully-stretched configurations, while **O*m*** shows a slightly higher conductance for the most probable conductance extracted from conductance histogram.

The key results of the MCBJ measurements are summarized in Table 1 and the corresponding original results are presented in the Supporting Information (Supplementary Figures 24-33). No multiple features were observed in the experiments, including **3-O*p*** and **8-O*m***. The lower peaks covered by the grey area below 10^{-7} G_0 is the noise level of the MCBJ experiments (Figure 3(c and d)). All the curves were used for the statistical analysis without any data selection. Junction formation probability (JFP) is the proportion of molecular stretching traces with a pronounced plateau relative to the total number of traces (Table 1). It is judged by area ratio of the peak in the plateau length distribution. Direct tunneling traces have no plateau and decay faster to the noise level, corresponding to the smaller stretching peak alongside the molecular peak in the plateau length histogram. (Supplementary Figures 24-33).

Several interesting conclusions can be drawn from the comparative conductance values of these molecules. First, in all cases, molecules with *para* connectivity **1–5** present larger conductance values than their *meta*

isomers, regardless of the bridging unit. This can be attributed to the partial de Broglie waves traversing in different paths through the core being in phase in the *para* isomers, giving rise to a constructive quantum interference (QI) effect. On the contrary, in the *meta*-anchored isomers the waves are out of phase leading to destructive quantum interference. The conductance relationship of the *para* and *meta* molecules is consistent with that of molecules with a central single benzene ring[27–29,43], indicating the quantum interference effect can still operate in polycyclic compounds. Secondly, the structure of the central core plays an important role in the conductance of QI molecules. It is noted that the largest difference between the *para*– and *meta*–anchored molecules (ΔG) is for the dibenzofuran pair **3-O*p*** and **8-O*m***, 1.37 $\log(G/G_0)$. However, as we reported previously, the differences between *para* and *meta* linked molecules are nearly 1.50 $\log(G/G_0)$ in benzene-cored analogs[29]. The lower experimental differences in the present study demonstrate that the quantum interference effect has not been amplified, and is even slightly reduced, by bridging the two benzene rings with a five-membered ring. Additionally, differences of the conductance in fully-stretched conformations between *para*– and *meta*–anchored molecules follow the increasing order of ΔG**C** < ΔG**N** < ΔG**S** < ΔG**O**, illustrating that the heteroatom can also contribute to the expression of the quantum interference. The electrode separations (z_{exp} in Table 1) are in good agreement with the theoretical molecular lengths. This indicates that in the fully stretched configuration, the molecular junctions are primarily linked by the gold–nitrogen bonds.

Moreover, there is no distinct correlation between the plateau length (or JFP) and the nature of the bridging atoms (S, N, O or C), demonstrating that these atoms have no significant influence on the conformation of the molecular junction. Furthermore, we did not observe any additional conductance group during the experiments for the ten molecules. We attributed this fact to three reasons. Firstly, pyridyl-terminated compounds have been reported to show well-defined peaks in the conductance histograms resulting from the high directionality of the donor-acceptor binding between N lone pair and Au[15,44,45]. Secondly, the alkyl groups connected to the bridged atom (N and C) sterically hinder the interaction between the electrode and the core of the molecule as well as restricting any π-π interaction of two molecules. Thirdly, molecules with similar core structures have been reported[19,22,23] to exhibit only one conductance statistical peak, suggesting that the junction formed by the core of the molecule is not robust enough during the elongation process. In the control experiments with **5-2H*p*** and **10-2H*m***, however, we observed such an obvious difference that the conductance of **5-2H*p*** is higher than that of **10-2H*m*** by almost two orders of magnitude.

Theory and Simulations. To understand the effect of pendant groups on quantum interference in the molecules of Figure 1, we first consider their two tight-binding representations shown in Figure 4, connected to 1-dimensional external leads.

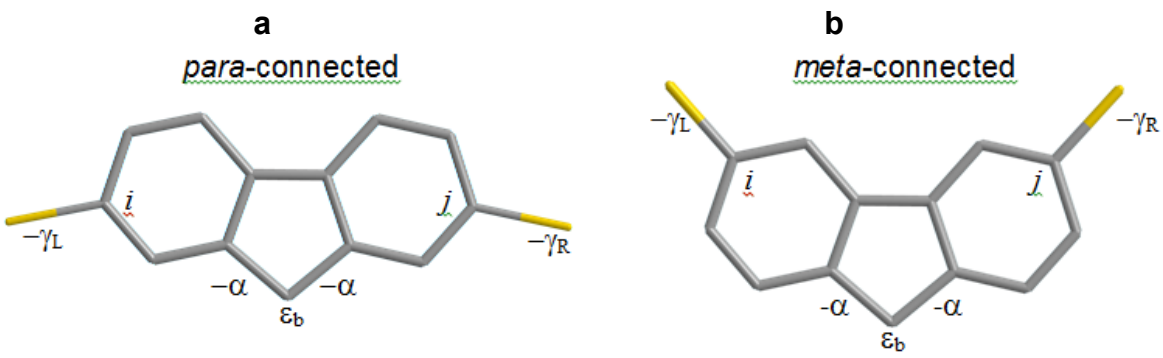

Figure 4 | Tight-binding (i.e. Hückel) models of *para*-(a) and *meta*-connected (b) molecules. Within the core of each, all site energies are zero except the pendant site energy ε_b and all nearest neighbour bonds are equal to –1, except for those denoted as α**.** The weaker couplings between the molecule and left leads are $-\gamma_L$ = -0.08 at atom number i and right leads $-\gamma_R$ = -0.08 at atom number *j*.

The tight binding model is introduced to illustrate the underlying trends in the transmission function and to allow us to obtain an analytic formula. Figure 5 shows results for various values of alpha, to reveal the evolution of the transmission curves with increasing coupling to the pendant groups. In Figure 6a, to use the simplest possible description, the same value of alpha = 1 is used for all molecules (for more information see Supplementary Table 5). When $\alpha = 0$, the pendant orbital is decoupled from the central core. Since the latter is a bipartite lattice, in the *meta* case, destructive interference should occur at the centre of the HOMO–LUMO gap (i.e. $E = 0$)[11,30,31]. The black curves in Figure 5 show the resulting transmission coefficients T (E), when $\varepsilon_b = 0$. The other curves in Figure 5 show how the transmission coefficient evolves as the coupling α to the pendant orbital is increased from zero (black curves) to unity (red curves).

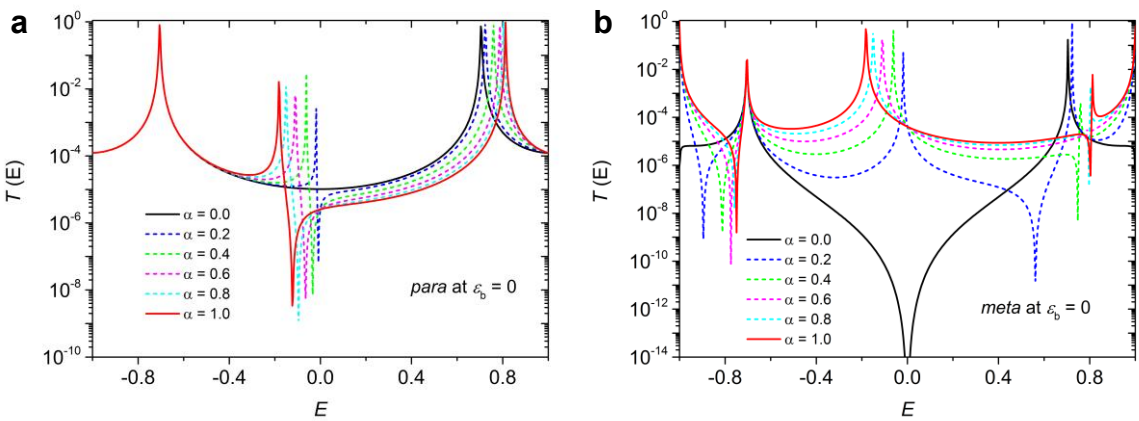

Figure 5 | *T* (E) vs. *E* for different values of α at ε_b = 0. Transmission coefficients *T* (E) for *para*-connection (a) and *meta*-connection (b), when ε_b = 0.

The above results show that in the absence of pendant groups (i.e. when $\alpha = 0$) the *meta* case shows a sharp transmission dip due to destructive interference at the gap centre, which is absent in the *para* case. In the presence of pendant groups (i.e. when α is non-zero) this destructive interference is alleviated in the *meta* case. In the *para* case, the non-zero coupling to the pendant group introduces a new conductance pathway, which can

cause destructive interference within the gap, signaled by the Fano lineshape just below $E = 0$. Further examples of this evolution for different choices of ε_b are presented in the SI. For the values of ε_b shown in Supplementary Table 5, Figure 6a, shows the resulting tight-binding transmission coefficients. Clearly the tight-binding model captures the qualitative features of the full density-functional calculation of transmission curves shown in Figure 6b. In particular the tight-binding result for **2-H*m***, which does not possess a pendant orbital, shows a pronounced transmission dip near $E = 0$, which is reflected in the low transmission coefficient predicted by DFT. (In the latter case, the presence of non-*pi* orbitals provides a parallel conductance path, which prevents the transmission coefficient completely vanishing.)

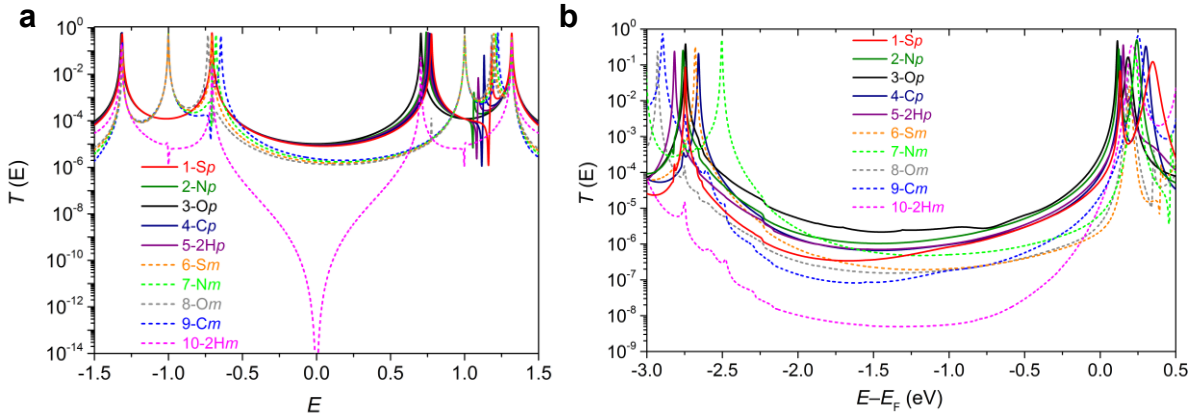

Figure 6 | Transmission coefficients. Results for the tight-binding (Hückel-model) transmission coefficients (**a**) obtained using the parameters in Supplementary Table 5. The transmission coefficients (**b**) obtained for electrodes with adatoms (see figure 7b) using density functional theory combined with Gollum.

The electronic interference structure calculations leading to transmission curves (Figure 6b) were performed using the DFT code SIESTA[46]. The optimum geometry of the isolated molecules was obtained by relaxing the molecules until all forces on the atoms were <0.05 V/Å. The SIESTA calculations employed a double-zeta plus polarization orbital basis set, norm-conserving pseudopotentials, an energy cutoff of 200 Rydbergs defined the real space grid and the exchange correlation functional was Local Density Approximation (LDA)[47].

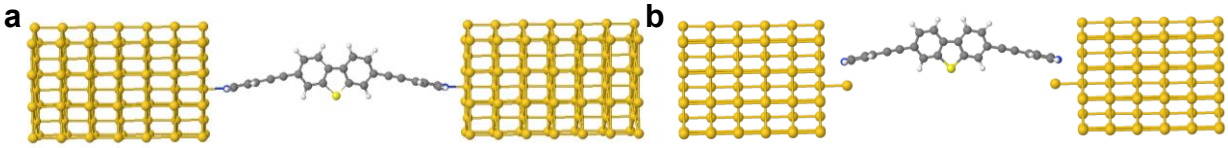

Figure 7| Geometry of the molecular junction containing a 1-S wire (a) on flat electrodes (b) on electrodes containing adatoms.

To calculate the conductance through these two groups of molecules, *para* and *meta* shown in Figure 1, they were attached to gold leads via the pyridyl anchor groups. The leads were constructed of 6 layers of (111) gold each containing 30 gold atoms. Transport calculations were carried out both for flat electrodes and for electrodes containing adatoms, as shown in Figure 7. According to DFT, the molecule binds most favourably to a top site, with a binding energy of about 0.8 eV at a distance of 2.3 Å (Figure 7 and Supplementary Figure 34-35) between the terminal nitrogen atoms and a 'top' gold atom. This most-favourable binding geometry has been

used in all simulations. A Hamiltonian describing this structure was produced using SIESTA and the zero-bias transmission coefficients $T(E)$ were calculated using the Gollum code[48]. An excellent agreement between theoretical and experimental conductance values has been obtained (Figure 8), by choosing a Fermi energy of E_F = –0.8 eV relative to the DFT-predicted value. Supplementary Figure 49 shows that the transmission coefficients of *meta*-connected molecules are all lower than those of *para* connected molecules over a wide energy range within their HOMO–LUMO gaps, in agreement with a tight-binding model of *pi*-orbital transport (Supplementary Figures 44–48). In the latter case, in the absence of bridging atoms (**5-2H*p*** and **10-2H*m***) there appear sharp transmission dips due to destructive interference in the *meta* case, which are alleviated by the presence of pendant groups. In contrast, in the *para* case, constructive interference in the *pi*-channel is preserved in the presence of bridging atoms. On the other hand, in the DFT-based transmission curves perfect destructive interference is masked by the presence of sigma orbitals, which provide a parallel path for conductance.

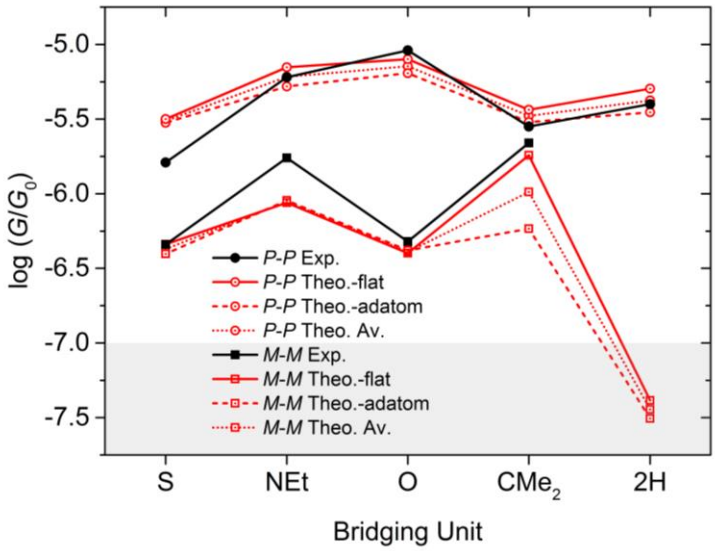

Figure 8 | Comparison between theoretical and experimental data for most probable conductance values. DFT results are shown for both flat electrodes (solid red lines) and with electrodes containing adatoms (dashed red lines). The dotted lines show the average of the 'flat' and 'adatom' DFT conductances. Although there are differences, we conclude that the same qualitative trends are obtained using both geometries, with the exception of CMe_2, which in the presence of adatoms, no longer has an anomalously high conductance observed experimentally in the *meta* case **9-C*m***.

Discussion

We conclude, therefore, from our experimental and theoretical data for the *para* series **1–4** and the *meta* series **6–9**, that there is a clear correlation between aromaticity of the central ring when heteroatoms are present and the single-molecule conductance value in the *para* series. Aromaticity follows the sequence: S > NEt > O > CMe_2. Our conductance trend for the heterocyclic *para* series, i.e. O > NEt > S is in agreement with a previous experimental study by Venkataraman, Breslow, et al[24] on monocyclic core units (furan > thiophene) (Figure 2). However, the fluorene derivative **4-C*p*** (which does not have a heteroatom in the core) shows a lower conductance than **2-N*p*** and **3-O*p*** although it exhibits a non-aromatic core. The reason for this exceptional behaviour of **4-C*p*** is not clear. However, we note that other workers[21–23] have observed that the single-molecule conductance of fluorene-based cores do not follow expected trends.

These results demonstrates that a non-aromatic core unit does not necessarily lead to higher conductance since the polycyclic series **1–5** exhibits a clear difference in comparison to the monocyclic series shown in Scheme 2. However, our data show that the sequence is very different in the *meta* series where dibenzothiophene ≈ dibenzofuran < carbazole. Multiple factors (such as quantum interference, aromaticity and electronegativity) and their composite effects should be taken into consideration in explaining the trends in the conductance. Our results show that bridging heteroatoms alleviate destructive quantum interference in the *meta*-connected molecules. The contribution of electronegativity of the bridging atoms should not be ignored. For the *meta* series dibenzothiophene **6-S*m*** and dibenzofuran **8-O*m*** represent both extremes. Dibenzothiophene **S*m*** is the most aromatic and therefore it lowers the conductance. As was mentioned above, dibenzofuran **8-O*m*** is the least aromatic core unit. Therefore, based on the conclusions of the series shown in Figure 2, **8-O*m*** should be the most conductive molecule. However, the lone pair of oxygen is tightly bonded due to oxygen's high electronegativity, which hinders the delocalization of electrons and decreases the electron density of the conjugated π system in **8-O*m***. The carbazole derivative **7-N*m*** is the most conductive in this *meta* series because it is less aromatic than dibenzothiophene, but also bears a lone pair which allows transmission through the molecule. The conductance of model non-bridged compound **5-2H*p*** is reduced because of the dihedral angle between the two phenyl units. Model compound **10-2H*m*** shows no conductance within the detection limit of the MCBJ setup. This is consistent with the bridging atom of **6-9** planarizing the core, which is essential for raising the conductance in the *meta*-series.

We have studied the single-molecule conductance of ten oligo(arylene-ethynylene) derivatives with five different core units (dibenzothiophene, carbazole, dibenzofuran, fluorene and biphenyl) attached to gold electrodes by pyridyl anchoring groups. Within the two series there is either *para-para* or *meta-meta* conjugation through the core unit. In all cases molecules with *para* connectivity present larger conductances than their *meta* isomers, regardless of the bridging unit. We have experimentally and theoretically observed clear and distinct trends in the *para* and *meta* series. In the *para* series there is a clear correlation between aromaticity of the central ring and the single-molecule conductance values in the sequence dibenzofuran > carbazole > dibenzothiophene, in agreement with a previous experimental study on monocyclic core units (furan > thiophene). However, in the *meta* series the carbazole derivative is the most conductive: the sequence dibenzothiophene ≈ dibenzofuran < carbazole. It is concluded that the nitrogen lone pair facilitates transmission through the molecule. Overall, we find that constructive quantum interference in the *para*-connected molecules persists in the presence of bridging atoms and is partly masked by the presence of sigma channels, whereas bridging atoms alleviate destructive quantum interference in the *meta*-connected molecules. Our comprehensive study establishes that both quantum interference and heteroaromaticity in the molecular core units play important and inter-related roles in determining the conductance of single molecular junctions. These results should assist in future research in the development of new molecules for incorporation into nanoscale molecular circuits.

Methods

Synthesis. Details of the synthesis and molecular characterization are in the Supplementary Notes 1–2.

MCBJ measurements.

Electron transport characteristics in single-molecule junctions were studied by MCBJ measurements in solution at room temperature. The molecular solution contained typically 0.1 mM of the **1–10** molecules in a mixture of 1,3,5-trimethylbenzene (Aldrich, p.a.) and tetrahydrofuran (Aldrich, p.a.), 4:1 (v/v). Single-molecule conductance experiments were performed during the formation and breaking of a nanogap on a notched, freely suspended gold wire (0.1 mm diameter, 99.999%, Goodfellow) fixed on spring steel sheets (10 mm × 30 mm, 0.25 mm thick) with a two-component epoxy glue (Stycast 2850 FT with catalyst 9). A Kel-F liquid cell with a Kalrez O-ring was mounted onto the sample sheet fixed by two holders. During the measurements, the steel sample could be bent with a pushing rod controlled by a stepper motor (or a piezo motor) and a piezo stack. The stepper motor initialized the bending process. Once the measured current reached a value corresponding to 15 G_0, the stepper motor paused and the piezo stack was activated. This strategy managed to decrease environmental noise significantly from the operation of the stepper motor. After the junction was completely opened, the piezo stack was reset and the stepper motor drove down the pushing rod. The movement of the piezo stack controlled the breaking and the reformation of nanoscale contacts and the stretching rate of the two gold leads controlled by the piezo stack is about 5–20 nm/s. Molecular junctions could form upon breaking the gold–gold nanocontacts. More than 1000 conductance–distance curves were recorded for statistically relevant data analysis during the repeated cycles.

The MCBJ controller is based on a laboratory-built bipotentiostat. All current measurements were performed with two custom-designed bipolar and tunable logarithmic I–V converters operating in a wide dynamic range from 10 to below 10^{-7} G_0. The tunneling current between the two ends of the 'broken wire' (taken as WE1 and WE2) could be recorded as a feedback signal at a given bias voltage 0.1 V. The distance between the two gold electrodes in the MCBJ setup is calibrated by the STM-BJ setup with the assumption that the tunneling decay is identical under the same experimental conditions. After breaking a gold-gold contact, the conductance of the junction drops to approximately 10^{-3} G_0. Due to the so-called "snap-back" effect, the gap between the two gold electrodes increases instantaneously to a certain distance Δz_{corr}. A perfect linear atomic chain of gold has a conductance of G_0. Due to the tunneling theory, we assume that $\log (G/G_0) = -\alpha z_{exp}$, where $z_{exp} = 0$ corresponds to the point where the distance between the terminating gold atoms is equal to the equilibrium gold-gold separation. Our measured separation is $\Delta z = z_{exp} - \Delta z_{corr}$, where Δz_{corr} is the snap-back distance. Then, the relationship between $\log (G/G_0)$ and Δz is $\log (G/G_0) = -\alpha\Delta z - \alpha\Delta z_{corr}$. The $\log(G/G_0)$ plot has a slope of $-\alpha$ and an intercept of $-\alpha\Delta z_{corr}$. To calibrate the stretching distance in the absence of molecules, we measured the conductance G versus Δz for conductances ranging from 10^{-4} to 10^{-6} G_0 and extracted the slope and intercept. From repeated measurements, we obtained a distribution of slopes and intercepts and from the most probable slopes and intercepts obtained the most probable values of α and Δz_{corr}. We concluded from individual experiments that in TMB: THF (v:v = 4:1), the Δz_{corr} is determined as 0.5 nm and the addition of a low concentration of molecules in solution does not influence the snap-back distance. Further technical details and data evaluation methods have been described in our previous article by Hong et al[49].

Theory and simulations. Details of the theory and simulations are in Supplementary Notes 4-5.

References

1. Carroll, R. L. & Gorman, C. B. The Genesis of Molecular Electronics. *Angew. Chem. Int. Ed.* **41,** 4378–4400 (2002).
2. Chen, F., Hihath, J., Huang, Z., Li, X. & Tao, N. J. Measurement of Single-Molecule Conductance. *Annu. Rev. Phys. Chem.* **58,** 535–564 (2007).
3. Moth-Poulsen, K. & Bjørnholm, T. Molecular electronics with single molecules in solid-state devices. *Nat. Nanotechnol.* **4,** 551–556 (2009).
4. Cuevas, J. C. & Scheer, E. *Molecular Electronics: An Introduction to Theory and Experiment*. (WORLD SCIENTIFIC, 2010).
5. Leary, E. *et al.* Incorporating single molecules into electrical circuits. The role of the chemical anchoring group. *Chem. Soc. Rev.* **44,** 920–942 (2015).
6. Perrin, M. L., Burzurí, E. & van der Zant, H. S. J. Single-molecule transistors. *Chem. Soc. Rev.* **44,** 902–919 (2015).
7. Song, H., Reed, M. A. & Lee, T. Single Molecule Electronic Devices. *Adv. Mater.* **23,** 1583–1608 (2011).
8. Weibel, N., Grunder, S. & Mayor, M. Functional molecules in electronic circuits. *Org. Biomol. Chem.* **5,** 2343–2353 (2007).
9. Reed, M. A., Zhou, C., Muller, C. J., Burgin, T. P. & Tour, J. M. Conductance of a Molecular Junction. *Science* **278,** 252–254 (1997).
10. Xu, B. & Tao, N. J. Measurement of Single-Molecule Resistance by Repeated Formation of Molecular Junctions. *Science* **301,** 1221–1223 (2003).
11. Lambert, C. J. Basic concepts of quantum interference and electron transport in single-molecule electronics. *Chem. Soc. Rev.* **44,** 875–888 (2015).
12. Tour, J. M. *et al.* Synthesis and Preliminary Testing of Molecular Wires and Devices. *Chem. – Eur. J.* **7,** 5118–5134 (2001).
13. Huber, R. *et al.* Electrical Conductance of Conjugated Oligomers at the Single Molecule Level. *J. Am. Chem. Soc.* **130,** 1080–1084 (2008).
14. Kaliginedi, V. *et al.* Correlations between Molecular Structure and Single-Junction Conductance: A Case Study with Oligo(phenylene-ethynylene)-Type Wires. *J. Am. Chem. Soc.* **134,** 5262–5275 (2012).
15. Zhao, X. *et al.* Oligo(aryleneethynylene)s with Terminal Pyridyl Groups: Synthesis and Length Dependence of the Tunneling-to-Hopping Transition of Single-Molecule Conductances. *Chem. Mater.* **25,** 4340–4347 (2013).

16. González, M. T. *et al.* Stability of Single- and Few-Molecule Junctions of Conjugated Diamines. *J. Am. Chem. Soc.* **135,** 5420–5426 (2013).

17. Jenny, N. M., Mayor, M. & Eaton, T. R. Phenyl–Acetylene Bond Assembly: A Powerful Tool for the Construction of Nanoscale Architectures. *Eur. J. Org. Chem.* **2011,** 4965–4983 (2011).

18. Eicher, T., Hauptmann, S. & Speicher, A. in *The Chemistry of Heterocycles* 52–121 (Wiley-VCH Verlag GmbH & Co. KGaA, 2003).

19. Venkataraman, L., Klare, J. E., Nuckolls, C., Hybertsen, M. S. & Steigerwald, M. L. Dependence of single-molecule junction conductance on molecular conformation. *Nature* **442,** 904–907 (2006).

20. Haiss, W. *et al.* Variable contact gap single-molecule conductance determination for a series of conjugated molecular bridges. *J. Phys. Condens. Matter* **20,** 374119 (2008).

21. Vonlanthen, D. *et al.* Chemically Controlled Conductivity: Torsion-Angle Dependence in a Single-Molecule Biphenyldithiol Junction. *Angew. Chem. Int. Ed.* **48,** 8886–8890 (2009).

22. Mishchenko, A. *et al.* Influence of Conformation on Conductance of Biphenyl-Dithiol Single-Molecule Contacts. *Nano Lett.* **10,** 156–163 (2010).

23. Mishchenko, A. *et al.* Single-Molecule Junctions Based on Nitrile-Terminated Biphenyls: A Promising New Anchoring Group. *J. Am. Chem. Soc.* **133,** 184–187 (2011).

24. Chen, W. *et al.* Aromaticity Decreases Single-Molecule Junction Conductance. *J. Am. Chem. Soc.* **136,** 918–920 (2014).

25. Klausen, R. S. *et al.* Evaluating atomic components in fluorene wires. *Chem. Sci.* **5,** 1561–1564 (2014).

26. Meisner, J. S. *et al.* Importance of Direct Metal−π Coupling in Electronic Transport Through Conjugated Single-Molecule Junctions. *J. Am. Chem. Soc.* **134,** 20440–20445 (2012).

27. Arroyo, C. R. *et al.* Quantum interference effects at room temperature in OPV-based single-molecule junctions. *Nanoscale Res. Lett.* **8,** 234 (2013).

28. Arroyo, C. R. *et al.* Signatures of Quantum Interference Effects on Charge Transport Through a Single Benzene Ring. *Angew. Chem. Int. Ed.* **52,** 3152–3155 (2013).

29. Manrique, D. Z. *et al.* A quantum circuit rule for interference effects in single-molecule electrical junctions. *Nat. Commun.* **6,** 6389 (2015).

30. Sangtarash, S. *et al.* Searching the Hearts of Graphene-like Molecules for Simplicity, Sensitivity, and Logic. *J. Am. Chem. Soc.* **137,** 11425–11431 (2015).

31. Geng, Y. *et al.* Magic Ratios for Connectivity-Driven Electrical Conductance of Graphene-like Molecules. *J. Am. Chem. Soc.* **137,** 4469–4476 (2015).

32. Liu, X. *et al.* A 2,7-carbazole-based dicationic salt for fluorescence detection of nucleic acids and two-photon fluorescence imaging of RNA in nucleoli and cytoplasm. *Org. Biomol. Chem.* **9,** 3615–3618 (2011).

33. Singh, V., Wang, S. & Kool, E. T. Genetically Encoded Multispectral Labeling of Proteins with Polyfluorophores on a DNA Backbone. *J. Am. Chem. Soc.* **135,** 6184–6191 (2013).

34. Dias, F. B. *et al.* Dipolar Stabilization of Emissive Singlet Charge Transfer Excited States in Polyfluorene Copolymers. *J. Phys. Chem. B* **112,** 6557–6566 (2008).

35. Wang, S. *et al.* Dicationic dibenzofuran derivatives as anti-Pneumocystis carinii pneumonia agents: synthesis, DNA binding affinity, and anti-P. carinii activity in an immunosuppressed rat model. *Eur. J. Med. Chem.* **34,** 215–224 (1999).

36. Esra Oğuztürk, H., Tirkeş, S. & Önal, A. M. Electrochemical synthesis of new conjugated polymers based on carbazole and furan units. *J. Electroanal. Chem.* **750,** 1–8 (2015).

37. Kobin, B., Grubert, L., Blumstengel, S., Henneberger, F. & Hecht, S. Vacuum-processable ladder-type oligophenylenes for organic–inorganic hybrid structures: synthesis, optical and electrochemical properties upon increasing planarization as well as thin film growth. *J. Mater. Chem.* **22,** 4383–4390 (2012).

38. Yang, W. *et al.* Improvement of color purity in blue-emitting polyfluorene by copolymerization with dibenzothiophene. *J. Mater. Chem.* **13,** 1351–1355 (2003).

39. Maji, M. & Studer, A. Transition-Metal-Free Oxidative Homocoupling of Aryl, Alkenyl, and Alkynyl Grignard Reagents with TEMPO. *Synthesis* **2009,** 2467–2470 (2009).

40. Holmes, B. T., Pennington, W. T. & Hanks, T. W. Efficient Synthesis of a Complete Donor/Acceptor bis(Aryl)diyne Family. *Synth. Commun.* **33,** 2447–2461 (2003).

41. Moreno-García, P. *et al.* Single-Molecule Conductance of Functionalized Oligoynes: Length Dependence and Junction Evolution. *J. Am. Chem. Soc.* **135,** 12228–12240 (2013).

42. Hong, W. *et al.* Single Molecular Conductance of Tolanes: Experimental and Theoretical Study on the Junction Evolution Dependent on the Anchoring Group. *J. Am. Chem. Soc.* **134,** 2292–2304 (2012).

43. Kiguchi, M., Nakamura, H., Takahashi, Y., Takahashi, T. & Ohto, T. Effect of Anchoring Group Position on Formation and Conductance of a Single Disubstituted Benzene Molecule Bridging Au Electrodes: Change of Conductive Molecular Orbital and Electron Pathway. *J. Phys. Chem. C* **114,** 22254–22261 (2010).

44. Wu, S. *et al.* Molecular junctions based on aromatic coupling. *Nat. Nanotechnol.* **3,** 569–574 (2008).

45. Frisenda, R. *et al.* Electrical properties and mechanical stability of anchoring groups for single-molecule electronics. *Beilstein J. Nanotechnol.* **6,** 1558–1567 (2015).

46. Soler, J. M. *et al.* The SIESTA method for ab initio order- N materials simulation. *J. Phys. Condens. Matter* **14,** 2745 (2002).

47. Langreth, D. C. & Perdew, J. P. Exchange-correlation energy of a metallic surface: Wave-vector analysis. *Phys. Rev. B* **15,** 2884–2901 (1977).

48. Ferrer, J. *et al.* GOLLUM: a next-generation simulation tool for electron, thermal and spin transport. *New J. Phys.* **16,** 093029 (2014).

49. Hong, W. *et al.* An MCBJ case study: The influence of π-conjugation on the single-molecule conductance at a solid/liquid interface. *Beilstein J. Nanotechnol.* **2,** 699–713 (2011).

Acknowledgments

We thank EC FP7 ITN 'MOLESCO' project number 606728 for funding work in Durham, Lancaster and Bern; UK EPSRC grants EP/M014452/1, EP/N017188/1, EP/K039423/1 and EP/L02621X/1 for funding work in the UK. Thousand youth talents plan of China, and national natural science foundation of China (2162780023) for funding work in Xiamen. A.A.A. acknowledges financial support from University of Anbar. L.W. acknowledges the Chinese Scholarship Council for financial support.

Author contributions

M.G., L.W. and A.A.A. contributed equally to the work in this manuscript. All authors have given approval to the final version of the manuscript. All authors provided essential contributions to interpreting the data reported in this manuscript. M.R.B., C.J.L and W.H. originally conceived the concept and designed the experiments. Synthetic work was carried out in M.R.B.'s laboratory by M.G.; break junction measurements were carried out in W.H.'s laboratory by L.W.; calculations were carried out in C.J.L.'s laboratory by A.A.A. and A.K.I.. M.G. coordinated the writing of the manuscript with input from all authors.

Corresponding Author

Correspondence and requests for materials should be addressed to M.R.B. (email: m.r.bryce@durham.ac.uk) or to W.H. (email: whong@xmu.edu.cn) or to C.J.L. (email: c.lambert@lancaster.ac.uk).

Supplementary Information. Synthetic procedures, characterization data; UV–Vis absorption; NMR spectra; and MCBJ conductance analysis of compounds **1**–**10**; additional theoretical data.

Competing financial interests. The authors declare no competing financial interests.